



Sublattice symmetry breaking and ultralow energy excitations in graphene-on-*h*BN heterostructures

U. R. Singh,¹ M. Prada,^{2,*} V. Strenzke,¹ B. Bosnjak,¹ T. Schmirander^{1,2},,² L. Tiemann¹,,¹ and R. H. Blick^{1,†}

¹*Center for Hybrid Nanostructures (CHyN), University of Hamburg, Luruper Chaussee 149, 22607 Hamburg, Germany*

²*Institute for Theoretical Physics, University of Hamburg, Jungiusstrasse 9-11, 20355 Hamburg, Germany*



(Received 7 June 2020; revised 30 October 2020; accepted 25 November 2020; published 22 December 2020)

The low-lying states of graphene contain exciting topological properties that depend on the interplay of different symmetry-breaking terms. The corresponding energy gaps remained unexplored until recently due to the low-energy scale of the terms involved (few tens of μeV). These low-energy terms include sublattice splitting, the Rashba coupling, and the intrinsic spin-orbit coupling, whose balance determines the topological properties. In this work, we unravel the contributions arising from the sublattice and the intrinsic spin orbit splitting in graphene on hexagonal boron-nitride. Employing resistively detected electron spin resonance, we identify a sublattice splitting of the order of 20 μeV , and we confirm an intrinsic spin orbit coupling of approximately 45 μeV . The dominance of the latter suggests a topologically nontrivial state, involving fascinating properties. Electron spin resonance is a promising route toward unveiling the intriguing band structure at low-energy scales.

DOI: [10.1103/PhysRevB.102.245134](https://doi.org/10.1103/PhysRevB.102.245134)

I. INTRODUCTION

The most striking electronic properties of graphene are linked to the bipartite nature of the honeycomb lattice, consisting of two interpenetrating triangular sublattices. In idealized graphene with sublattice degeneracy, the electrons become chiral in the continuum limit [1]. The electrons can then be described by a Dirac Hamiltonian, which accounts for the absence of backscattering [2]. Atomic or more specifically intrinsic spin orbit coupling (SOC) breaks spin rotational symmetry, preserving chirality and opening a gap in the spectrum [3–5]. This gap transforms the system into a topological insulator that gives rise to the spin-Hall effect. Sublattice symmetry-breaking terms can preserve the topological properties as long as the splitting is compensated by the intrinsic SOC gap. Resolving the low-lying energetic bands in graphene is thus crucial in order to unveil the rich physics of Dirac charge carriers. We employ resistively detected electron spin resonance (RD-ESR) and access these low-lying bands.

Sublattice symmetry breaking in van der Waals (vdW) materials can arise due to coupling to the substrate [6,7]. An example for this is the encapsulation of the charge carrying material graphene with insulators, such as hexagonal boron nitride (*h*BN) [8–11]. Having a small lattice mismatch of about 1.8% between the two hexagonal lattices [6,9], the symmetry breaking favors energetically one of the two sublattices *A* and *B* in graphene on *h*BN (Go*h*BN) [6,7,10,12]. This can lead to the modification of the band structure including the opening of a gap, which remains an experimentally unexplored realm [6,7,13].

In this paper, we address the phenomenon of spin splitting of sublattices *A* and *B* in Go*h*BN, both theoretically and experimentally. We estimate the size of the splitting gap using resistively detected electron spin resonance at low temperatures. Our findings suggest the coexistence of intrinsic spin-orbit coupling and the spin splitting of sublattices with very small splitting gap values.

II. THEORETICAL DESCRIPTION

In the Dirac model, widely used to describe Dirac carriers in graphene [1,14], the notion of sublattice spin is introduced, where first-neighbor hopping is identified with a spin-flip operator. We describe the Hamiltonian using a minimal model in the bispinor basis spanned by spin and sublattice spin, $\{|\uparrow, \downarrow\rangle\} \otimes \{A, B\}$,

$$\hat{H} = \hbar v_F \mathbb{I} \otimes (\tau \hat{\sigma}_x k_x + \hat{\sigma}_y k_y) + \frac{1}{2} \Delta_I \tau \hat{\sigma}_z \otimes \hat{\sigma}_z + \frac{1}{2} \Delta_\gamma \hat{\sigma}_z \otimes \mathbb{I},$$

where Δ_I is the intrinsic SOC gap, Δ_γ is the sublattice splitting, τ is the valley index, and (k_x, k_y) is the small vector near the DP [1]. Without losing generality, we consider the case $\Delta_I > \Delta_\gamma$. In the absence of Rashba SOC, the conduction-band (CB) eigenstates near the *K* point ($\tau = 1, k_x = k_y = 0$) are $\{|\uparrow, A\rangle$ and $\{|\downarrow, B\rangle$ with energies $\Delta_I + \Delta_\gamma$ and $\Delta_I - \Delta_\gamma$, respectively, whereas the CB eigenstates at *K'* are $\{|\downarrow, A\rangle$ and $\{|\uparrow, B\rangle$, with energies $\Delta_I + \Delta_\gamma$ and $\Delta_I - \Delta_\gamma$.

Figure 1 shows schematically the band structure at both Dirac points (DPs), which are related by time inversion (and thus spin). The bands are colored according to the sublattice (blue for sublattice *A*, and magenta for sublattice *B*), and the spin eigenvalue s_z is denoted with an arrow. As a result of the chirality of graphene, the sublattice gap in neighboring DPs has the opposite sign. As a consequence, a magnetic field splits further the CB levels at one DP and reduces splitting at the other, that is, the splitting between CB spin up and down

*mprada@physnet.uni-hamburg.de

†Also at Materials Science and Engineering, University of Wisconsin–Madison, 1550 University Avenue, Madison, WI 53706, USA.

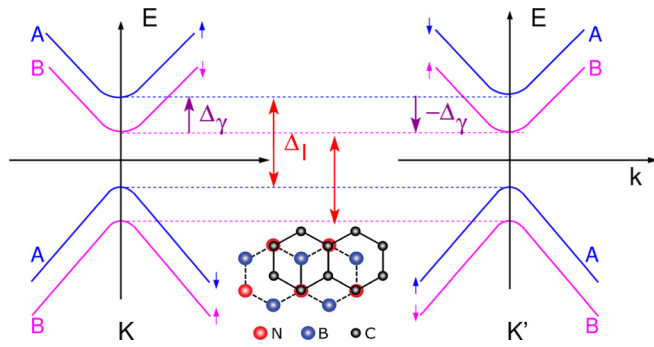


FIG. 1. Schematic band structure of the bulk bands near the DPs at $B = 0$ in the topological insulator condition: $\Delta_I > \Delta_\gamma$. The s_z eigenvalue of the bands is marked with an arrow, whereas the colors indicate sublattice degree of freedom: Blue for sublattice A and magenta for sublattice B. Inset: a case for boron (B) atoms of hBN situated at the center of the hexagonal lattice of graphene.

bands at either DP would be

$$\Delta_\epsilon^\pm = g\mu_B B \pm \Delta_\gamma. \quad (1)$$

Here, μ_B is the Bohr magneton and g is the g -factor, which is close to 1.95 in these experiments [5,15]. Our goal is to address these opposite-spin bands by employing RD-ESR, a method that had previously verified the existence of the intrinsic band gap in graphene [5,16]. This spin-sensitive probing technique allows us to resolve the energetic distance between spin bands, as the microwave excitation couples opposite spins [17]. We can detect the response to the resonant absorption of microwaves as changes in the resistivity in a Hall bar structure.

III. DEVICE FABRICATION AND EXPERIMENTAL METHODS

The $200 \mu\text{m} \times 22 \mu\text{m}$ GohBN-Hall bars were fabricated using chemical vapor deposition (CVD)-graphene and CVD-hBN on a highly p -doped silicon-on-insulator (SOI) substrate with a 285 nm top layer of SiO_2 . The CVD-hBN obtained on copper foil [18] was removed in iron nitrate solution, and after its transfer to the SOI, annealing was performed at $\sim 180^\circ\text{C}$ to ensure adhesion to the substrate [19,20]. We fabricate the Hall bar structure by transferring graphene onto the hBN and using optical lithography and ion etching, as described in detail elsewhere [21]. The resulting GohBN sample was thermally annealed at 350°C for 2 h to remove chemical residues remaining on the surface and in the vicinity of interfaces [9,22]. Metallic contacts were fabricated by depositing Ti/Au (7 nm/70 nm) via photolithography and physical vapor deposition.

To be able to resolve low energy excitations in the energy spectrum of graphene on hBN, we cooled the sample down to ~ 1.3 K in vacuum and used a low-frequency lock-in technique for the detection of the magnetoresistance and ESR under perpendicular magnetic fields (B). A back-gate voltage (V_{BG}) was applied to the substrate to vary the carrier concentration in the graphene layer and to shift the Fermi level closer to the DP. The microwaves are generated by a loop antenna placed next to the sample, as illustrated in Fig. 2(a).

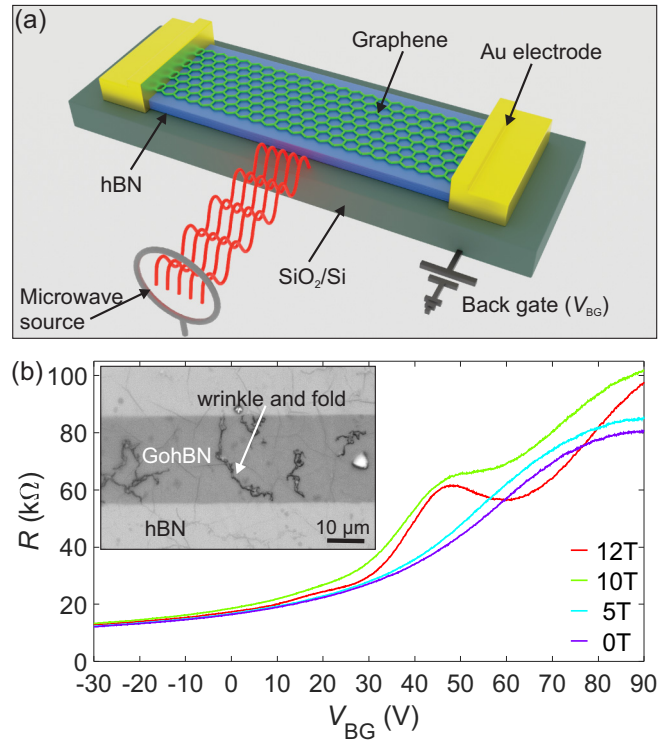


FIG. 2. (a) Schematic illustration of our $200 \mu\text{m} \times 22 \mu\text{m}$ GohBN Hall bar device and the loop antenna for microwave irradiation. (b) The apex of R vs V_{BG} at 90 V for $B = 0$ T marks the charge-neutrality point. Measurements at finite magnetic fields show the onset of Landau quantization. Inset: optical image of the GohBN Hall bar showing the surface of CVD graphene as a darker region.

Our graphene device is subject to unintentional doping; a back gate voltage of 90 V is required to access the charge neutrality point (CNP), seen as an apex in the two-terminal resistance [Fig. 2(b)]. A perpendicular B allows us to observe Landau quantization presented in the same figure. Further, we have extracted the carrier density n from the Hall measurement and obtained the carrier mobility (μ), which is of the order of $1200 \text{ cm}^2\text{V}^{-1}\text{s}^{-1}$. The poor mobility in our device can be limited by scattering on grain boundaries, wrinkles, and folds that are inherent to large-scale van der Waals materials synthesized by CVD and the transfer process [22,23,24]. The optical microscopic image in the inset of Fig. 2(b) visualizes some of these defects in our device.

We can identify low energy interband excitations between spin-split bands by probing the longitudinal sample resistance R_{xx} as a function of B in the absence (R_{xx}^{dark}) and in the presence (R_{xx}^{RF}) of microwave radiation of constant frequency. The microwave radiation thermally activates carriers, thus reducing the overall resistance as new channels for transport become available [25]. Whenever the microwave energy hf matches the energetic difference between two opposite spin polarized bands, an additional *resonant* interband excitation leads to a distinct peak in the photoinduced differential resistance $\Delta R = R_{xx}^{\text{dark}} - R_{xx}^{\text{RF}}$. We stress that the signal is nonlocal in the sense that it is sensitive to the enhanced density of states of dressed states, such as spin-split bands with a population imbalance.

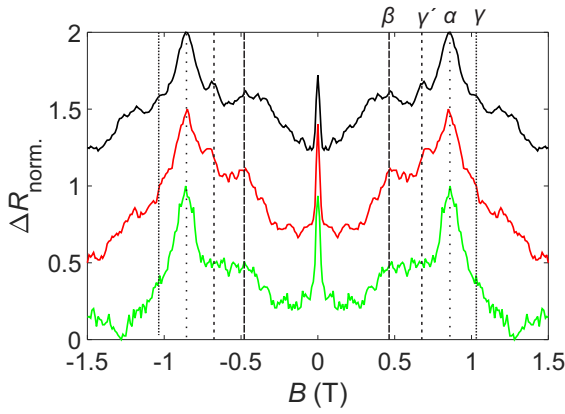


FIG. 3. Normalized curves of ΔR vs B at the exemplary frequency f of 23 GHz (21 dBm) plotted for $V_{BG} = 0$ V (green solid line), 50 V (red solid line), and 85 V (black solid line). Resonances between spin-split bands are labeled α , β , γ , and γ' . The vertical lines are a guide to the eye.

IV. RESULTS AND DISCUSSIONS

Figure 3 shows the resulting (normalized) resistance ΔR_{norm} as a function of B for an exemplary frequency f of 23 GHz, measured with $V_{BG} = 0$ V (i.e., energetically distant to the CNP), 50 V, and 85 V (i.e., energetically close to the CNP). ΔR_{norm} was obtained by normalizing each ΔR to the range 0–1. Resonant features are marked by dotted lines, and we introduce the labeling convention α , β , γ , and γ' to distinguish these resonances. We note that at this frequency, not all resonances are pronounced.

We have repeated the measurements at various constant frequencies. Figures 4(a)–4(c) show the derivative of the two-terminal resistance (dR/dB) in the f - B plane for $V_{BG} = 0$, 50, and 85 V, respectively. For 0 V in Fig. 4(a), at high carrier concentrations and energetically distant from the CNP, we only observe the linear dispersions of the α and β resonances. The linear extrapolation of α intercepts with the origin, suggesting that this line represents the ordinary Zeeman splitting. β intercepts with the f -axis at around 10 GHz and represents the intrinsic SOC gap [5]. α and β are accompanied by the satellite resonances γ and γ' , which intercept with the f -axis at $h^{-1}\Delta_\gamma < 0$ and $h^{-1}\Delta_{\gamma'} > 0$, respectively. This occurs for

$V_{BG} = 50$ and 85 V in Figs. 4(b) and 4(c), i.e., at lower carrier concentrations and energetically closer to the CNP, suggesting that Dirac electrons are responsible for the resonance.

The emergence of the γ and γ' lines strongly suggests a sublattice splitting according to Eq. (1) that is induced by the interaction with the h BN. The microwaves address these spin- and sublattice-split bands at low energies [13,26] and trigger additional interband excitations. We stress that extrinsic (i.e., Rashba) SOC contributions cannot account for the existence of γ and γ' . A hypothetical Rashba contribution would increase linearly with the electric field [27] from the back gate, and would *not* be symmetric with respect to α . According to Ref. [13], at least 5 V/nm are needed to observe extrinsic spin-orbit coupling effects. In contrast to reports using only h BN as a dielectric [28], the dielectric layer in our samples consists of h BN and almost 300 nm of Si oxide, which is too thick to generate high electric fields.

Likewise, magnetic impurities or adatoms can be ruled out. The zero-field splitting arising from magnetic adatoms is proportional to J_z^2 [29], and it would yield only one additional spectral line. Moreover, group symmetry considerations on a sixfold symmetric lattice forbid most electron-assisted transitions [30]. Under strain and to lowest order, an impurity would see a local C_6 point group that would not allow for the transitions we could detect.

We can obtain the spin- and sublattice-splitting energies by carefully analyzing the resonance occurrences presented in Fig. 4(c). Figure 5 shows the results of this analysis as frequency f versus the magnetic field occurrence of the resonance. A linear fit of the data points from α yields the slope $\Delta f/\Delta B = (26.68 \pm 0.48)$ GHz T $^{-1}$ and a g -factor of 1.90 ± 0.04 , which is consistent with previous reports on single and multilayer graphene on SiO $_2$ and SiC substrates [5,16]. We then use 1.90 ± 0.04 to linearly fit β , γ , and γ' and obtain the individual intercepts $h^{-1}\Delta$ with the frequency axis. The intercept times Planck's constant h yields the transition energies of $\Delta_I = (45.24 \pm 0.79)$ μ eV for β , $\Delta_{\gamma'} = (22.13 \pm 0.62)$ μ eV for γ' , and $\Delta_\gamma = (18.69 \pm 0.62)$ μ eV for γ .

We can now compare our results to anticipated interband transitions in graphene that are subject to spin *and* sublattice splitting, as illustrated in Fig. 1. The α and β resonances represent excitations between spin-split bands and across the intrinsic band gap, as previously reported [5]. The γ and γ'

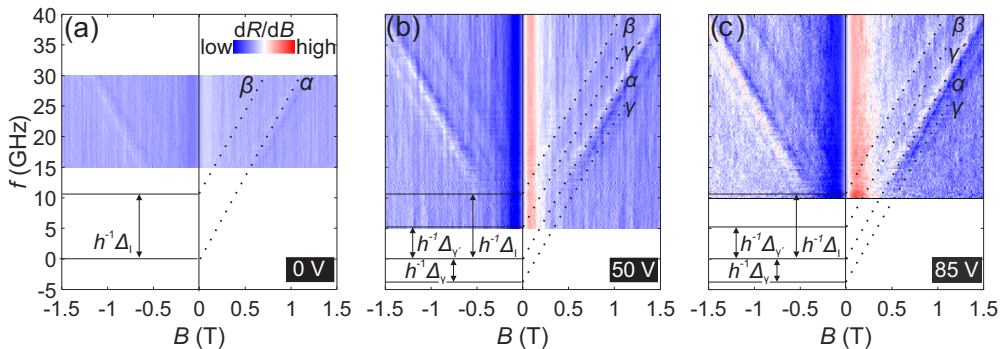


FIG. 4. dR/dB as a function of B and f for $V_{BG} = 0$ V (a), 50 V (b), and 85 V (c). α extrapolates to the origin in all measurements. β intensifies notably closer to the CNP, and the intercept of the β line with the f -axis represents intrinsic SOC. As a result of sublattice splitting, γ and γ' emerge out of the resistive background close to the CNP.

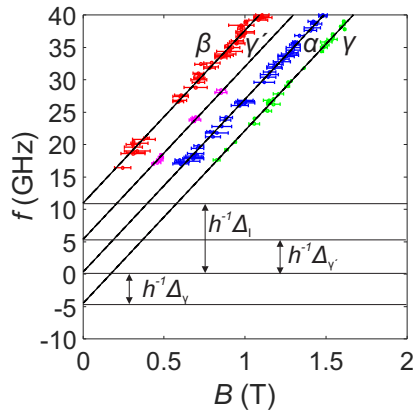


FIG. 5. Frequency vs absolute magnetic field, where resonances occurred, obtained by determining the zero-crossings of dR/dB from data in Fig. 4(c). The length of the error bars is estimated by taking the difference between the zero-crossing and maximum and minimum in the dR/dB curves. All black solid lines represent linear fits. The α fit yields a slope of $\Delta f/\Delta B = (26.68 \pm 0.48) \text{ GHz T}^{-1}$, or a g -factor of 1.90 ± 0.04 , respectively. This g -factor was used to fit β , γ , and γ' and obtain the intercepts with the f -axis of $h^{-1}\Delta_i \approx (10.94 \pm 0.19) \text{ GHz}$, $h^{-1}\Delta_{\gamma'} \approx (5.35 \pm 0.15) \text{ GHz}$, and $h^{-1}\Delta_{\gamma} \approx (-4.52 \pm 0.15) \text{ GHz}$.

spin resonances, however, can only occur when in addition to the lifting of the (electron) spin degeneracy, also the degeneracy of sublattices A and B is lifted.

We point out that the combination of monolayer graphene and boron nitride results in strong interactions between the two materials and in the emergence of moiré superlattices [9]. On a microscopic scale, the periodic potential created due to graphene superlattices can lead to a modification of the band structure at a low energy scale, giving rise to an asymmetry between the sublattices A and B and thus sublattice symmetry breaking [6,7,10–12]. The locations of B and N under carbon atoms of graphene play an important role in defining the sublattice splitting [13,26]. Van der Waals materials synthesized by CVD are comprised of many grains, and the randomized locations of the atoms are expected to result in some averaged value for the sublattice splitting. In our integrative measurement, we probe excitations within the resulting (macroscopic)

band structure, yielding a sublattice splitting to be of the order of $20 \mu\text{eV}$. A sublattice splitting smaller than an intrinsic SOC gap would indicate a nontrivial topological state [4]. In single crystalline samples [31], the sublattice splitting can be resolved in ordinary magnetotransport experiments. However, we use macroscopic polycrystalline samples in the continuum limit, where we have sensitivity to energies within the microwave range. Larger sublattice splittings would require higher frequencies.

For completion, we want to note that we also extracted the spin diffusion length [32,33] $\lambda_s = \sqrt{D\tau_s}$ from the α resonances in Fig. 4(c). Here, $D_s \simeq D$ is the spin diffusion constant, with $D = 0.5v_F l_{\text{mfp}} \simeq 1.1 \times 10^{-2} \text{ m}^2 \text{ s}^{-1}$. The spin relaxation time $\tau_s = \hbar(2h\frac{\Delta f}{\Delta B})^{-1}\delta B$, which is proportional to the resonance peak width (δB), gives τ_s in the range of $\sim(14\text{--}30) \text{ ps}$, corresponding to $\lambda_s \sim (385\text{--}558) \text{ nm}$.

V. CONCLUSION

In conclusion, our data indicate that the interaction between graphene and $h\text{BN}$ lifts the degeneracy of sublattices A and B . In our polycrystalline samples, the sublattice splitting energy is found to be of the order of $20 \mu\text{eV}$, which is dwarfed by the energetic resolution of most experimental techniques. However, the splitting must not be ignored since it competes in energy with the spin-orbit interaction. Our RD-ESR experiments can address the individual spin-split bands, giving us access to the realm of ultralow-energy scales and complex band structures that are subject to competing interactions.

ACKNOWLEDGMENTS

We acknowledge support by the Partnership for Innovation, Education, and Research (PIER). We also thank the Excellence Cluster Center for Ultrafast Imaging (CUI) of the Deutsche Forschungsgemeinschaft (DFG) for support under Contract No. EXC-1074. We are grateful to Jann Harberts for rendering the image shown in Fig. 2(a) with the BLENDER software. All measurements in this work were performed with NANOMEAS.

- [1] A. H. C. Neto, F. Guinea, N. M. R. Peres, K. S. Novoselov, and A. K. Geim, The electronic properties of graphene, *Rev. Mod. Phys.* **81**, 109 (2009).
- [2] M. I. Katsnelson, K. S. Novoselov, and A. K. Geim, Chiral tunneling and the Klein paradox in graphene, *Nat. Phys.* **2**, 620 (2006).
- [3] C. L. Kane and E. J. Mele, Quantum Spin Hall Effect in Graphene, *Phys. Rev. Lett.* **95**, 226801 (2005).
- [4] C. L. Kane and E. J. Mele, Z_2 Topological Order and the Quantum Spin Hall Effect, *Phys. Rev. Lett.* **95**, 146802 (2005).
- [5] J. Sichau, M. Prada, T. Anlauf, T. J. Lyon, B. Bosnjak, L. Tiemann, and R. H. Blick, Resonance Microwave Measurements of an Intrinsic Spin-Orbit Coupling Gap in Graphene: A

Possible Indication of a Topological State, *Phys. Rev. Lett.* **122**, 046403 (2019).

- [6] J. C. W. Song, A. V. Shytov, and L. S. Levitov, Electron Interactions and Gap Opening in Graphene Superlattices, *Phys. Rev. Lett.* **111**, 266801 (2013).
- [7] J. Jung, A. M. Dasilva, A. H. Macdonald, and S. Adam, Origin of band gaps in graphene on hexagonal boron nitride, *Nat. Commun.* **6**, 6308 (2015).
- [8] C. R. Dean, A. F. Young, I. Meric, C. Lee, L. Wang, S. Sorgenfrei, K. Watanabe, T. Taniguchi, P. Kim, K. L. Shepard, and J. Hone, Boron nitride substrates for high-quality graphene electronics, *Nat. Nanotechnol.* **5**, 722 (2010).
- [9] M. Yankowitz, J. Xue, D. Cormode, J. D. Sanchez-Yamagishi, K. Watanabe, T. Taniguchi, P. Jarillo-Herrero, P. Jacquod, and

- B. J. Leroy, Emergence of superlattice Dirac points in graphene on hexagonal boron nitride, *Nat. Phys.* **8**, 382 (2012).
- [10] B. Hunt, T. Taniguchi, P. Moon, M. Koshino, and R. C. Ashoori, Massive Dirac fermions and Hofstadter butterfly in a van der Waals heterostructure, *Science* **340**, 1427 (2013).
- [11] L. Wang, Y. Gao, B. Wen, Z. Han, T. Taniguchi, K. Watanabe, M. Koshino, J. Hone, and C. R. Dean, Evidence for a fractional fractal quantum Hall effect in graphene superlattices, *Science* **350**, 1231 (2015).
- [12] F. Amet, J. R. Williams, K. Watanabe, T. Taniguchi, and D. Goldhaber-Gordon, Insulating Behavior at the Neutrality Point in Single-Layer Graphene, *Phys. Rev. Lett.* **110**, 216601 (2013).
- [13] K. Zollner, M. Gmitra, and J. Fabian, Heterostructures of graphene and hBN: Electronic, spin-orbit, and spin relaxation properties from first principles, *Phys. Rev. B* **99**, 125151 (2019).
- [14] M. I. Katsnelson, *Graphene: Carbon in Two Dimensions* (Cambridge University Press, Cambridge, 2012).
- [15] T. J. Lyon, J. Sichau, A. Dorn, A. Centeno, A. Pesquera, A. Zurutuza, and R. H. Blick, Probing Electron Spin Resonance in Monolayer Graphene, *Phys. Rev. Lett.* **119**, 066802 (2017).
- [16] R. G. Mani, J. Hankinson, C. Berger, and W. A. De Heer, Observation of resistively detected hole spin resonance and zero-field pseudo-spin splitting in epitaxial graphene, *Nat. Commun.* **3**, 996 (2012).
- [17] C. P. Slichter, *Principles of Magnetic Resonance*, Springer Series in Solid-State Sciences Vol. 1 (Springer, Berlin, 1990).
- [18] 20-nm-thick CVD hBN purchased from Graphene Laboratories Inc., Ronkonkoma, NY, USA.
- [19] V. Shautsova, A. M. Gilbertson, N. C. G. Black, S. A. Maier, and L. F. Cohen, Hexagonal boron nitride assisted transfer and encapsulation of large area CVD graphene, *Sci. Rep.* **6**, 30210 (2016).
- [20] D. De Fazio, D. G. Purdie, A. K. Ott, P. Braeuninger-Weimer, T. Khodkov, S. Goossens, T. Taniguchi, K. Watanabe, P. Livreri, F. H. L. Koppens, S. Hofmann, I. Goykhman, A. C. Ferrari, and A. Lombardo, High-mobility, wet-transferred graphene grown by chemical vapor deposition, *ACS Nano* **13**, 8926 (2019).
- [21] T. J. Lyon, J. Sichau, A. Dorn, A. Zurutuza, A. Pesquera, A. Centeno, and R. H. Blick, Upscaling high-quality CVD graphene devices to 100 micron-scale and beyond, *Appl. Phys. Lett.* **110**, 113502 (2017).
- [22] S. M. Kim, A. Hsu, M. H. Park, S. H. Chae, S. J. Yun, J. S. Lee, D. H. Cho, W. Fang, C. Lee, T. Palacios, M. Dresselhaus, K. K. Kim, Y. H. Lee, and J. Kong, Synthesis of large-area multilayer hexagonal boron nitride for high material performance, *Nat. Commun.* **6**, 8662 (2015).
- [23] N. Petrone, C. R. Dean, I. Meric, A. M. van der Zande, P. Y. Huang, L. Wang, D. Muller, K. L. Shepard, and J. Hone, Chemical vapor deposition-derived graphene with electrical performance of exfoliated graphene, *Nano Lett.* **12**, 2751 (2012).
- [24] W. Zhu, T. Low, V. Perebeinos, A. A. Bol, Y. Zhu, H. Yan, J. Tersoff, and P. Avouris, Structure and electronic transport in graphene wrinkles, *Nano Lett.* **12**, 3431 (2012).
- [25] S. Datta, *Electronic Transport in Mesoscopic Systems* (Cambridge University Press, Cambridge, 1995).
- [26] A. W. Cummings, S. M. M. Dubois, J. C. Charlier, and S. Roche, Universal spin diffusion length in polycrystalline graphene, *Nano Lett.* **19**, 7418 (2019).
- [27] E. I. Rashba, Graphene with structure-induced spin-orbit coupling: Spin-polarized states, spin zero modes, and quantum Hall effect, *Phys. Rev. B* **79**, 161409(R) (2009).
- [28] L. Banszerus, B. Frohn, T. Fabian, S. Somanchi, A. Epping, M. Müller, D. Neumaier, K. Watanabe, T. Taniguchi, F. Libisch, B. Beschoten, F. Hassler, and C. Stampfer, Observation of the Spin-Orbit Gap in Bilayer Graphene by One-Dimensional Ballistic Transport, *Phys. Rev. Lett.* **124**, 177701 (2020).
- [29] D. Gatteschi, R. Sessoli, and J. Villain, *Molecular Nanomagnets* (Oxford University Press, New York, 2006).
- [30] M. Prada, The geometric phase of Z_n - and T-symmetric nanomagnets as a classification toolkit, *Sci. Rep.* **7**, 46614 (2017).
- [31] Y. Nam, J. Sun, N. Lindvall, S. J. Yang, D. Kireev, C. R. Park, W. W. Park, and A. Yurgens, Quantum Hall effect in graphene decorated with disordered multilayer patches, *Appl. Phys. Lett.* **103**, 233110 (2013).
- [32] M. V. Kamalakar, C. Groenveld, A. Dankert, and S. P. Dash, Long distance spin communication in chemical vapour deposited graphene, *Nat. Commun.* **6**, 6766 (2015).
- [33] M. Gurram, S. Omar, and B. J. Van Wees, Electrical spin injection, transport, and detection in graphene-hexagonal boron nitride van der Waals heterostructures: Progress and perspectives, *2D Mater.* **5**, 032004 (2018).